Micron 130 (2020) 102798

Contents lists available at ScienceDirect

Micron

journal homepage: www.elsevier.com/locate/micron

Fully-automatic defects classification and restoration for STM images

Xian-guang Fan[a,b], Yi Wu[a], Yu-Liang Zhi[a], Hong Xia[a], Xin Wang[a,b,*]

[a] Department of Instrumental and Electrical Engineering, Xiamen University, Xiamen, Fujian, 361005, PR China
[b] Fujian Key Laboratory of Universities and Colleges for Transducer Technology, Xiamen, Fujian, 361005, PR China

ARTICLE INFO

Keywords:
STM
Image processing
DCNN
Classification
Restoration
RPCA

ABSTRACT

The Scanning tunneling microscope (STM) is a micro instrument designed for surface morphology with nanometer precision. The restoration of the STM image defects usually needs human judgements and manual positioning because of the diversity of the morphology and the randomness of the defects. This paper provides a new fully-automatic method that combines deep convolutional neural classification network and unique restoration algorithms corresponding to different defects. Aimed at automatically processing compound defects in STM images, the method first predicts what kinds of defects a raw STM image has by a series of parallel binary classification networks, and then decides the process order according to the predicted labels, and finally restores the defects by corresponding global restoration algorithms in order. Experiment results prove the provided method can restore the STM images by self-judging, self-positioning, self-processing without any manual intervention.

1. Introduction

Scanning tunneling microscope (STM), which has the ability of direct atomic-precise surface structure determination of objects, was introduced by G.Binnig and H.Rohrer in 1983 (Binnig and Rohrer, 1983). Both of them were awarded by the Nobel Price in physics 1986 for the invention (Binnig and Rohrer, 1987). As a powerful imaging tool, STM has been widely applied in surface science (Binnig et al., 1983; Nguyen et al., 2018), material science (Kumar et al., 2018), chemistry (Kelty and Lieber, 1989), biology (Voelker et al., 1988) and nanotechnology (Rosei et al., 2003; Tapaszto et al., 2008), etc. However, the STM system needs very high stability to generate high quality images, just slight outside vibration, motor periodic vibration or control system hysteresis may cause defects in morphologies. Hence, image post-processing of STM morphology is a very significant issue for STM application. The common defects of STM images are image damages, periodic noise, blur, low-contrast and so on. Three typical and common types of STM image defects to be processed are long stripe, short sparse stripe and periodic noise, as presented in Fig. 1.

Long stripe and short sparse stripe are examples of local noise. Long stripe is usually caused by the pinpoint tinny shake when the whole precise mechanical system having outside disturbance. On account of the pinpoint scanning direction is horizontal, almost all long stripe defects present as horizontal linear stripes occupying the whole row or at least quarter. Short stripe is usually generated by system hysteresis before and after the pinpoint scanning to a raised surface topography. Short stripes appear abundantly and sparsely in an image. The randomness and quantity of these two defects make identification and positioning a very time-consuming and inefficient work. Because these two noises are related to 'mistakes' during scanning procedure, they have their own characteristics distinguished from real physical morphologies, which make the automatic recognition and restoration possible.

Periodic noise usually appears globally in an image, because of the periodic mechanical vibration causing by motor or refrigerant fan rotation. Several researchers have introduced some methods of restoring strict periodic noise. T.Y. Ji (Ji et al., 2007) used partial filter called optimal soft morphological filter (OSMF) to remove the sinusoidal noise in images. Hong-tao Li (Li et al., 2010) used adaptive mathematical morphological filter to remove periodic narrow bandwidth noise. However, the methods in time domain can only perform well in strict periodic noise, whereas the methods in frequency domain are more suitable for the generic periodic noise on the contrary. Payman Moallem (Moallem et al., 2013) introduced a novel adaptive Gaussian notch filter to remove striping or local periodic noise. Fr´ed´eric Sur (Sur and Grédiac, 2015) introduced an automated notch filter based on the expected power spectrum of images to remove the pseudo periodic noise. While on account of the diversity of the periodic noise, positioning the frequency content in the frequency map becomes a difficult and complex task.

* Corresponding author.
E-mail address: xinwang@xmu.edu.cn (X. Wang).

https://doi.org/10.1016/j.micron.2019.102798
Received 14 September 2019; Received in revised form 4 December 2019; Accepted 4 December 2019
Available online 05 December 2019
0968-4328/

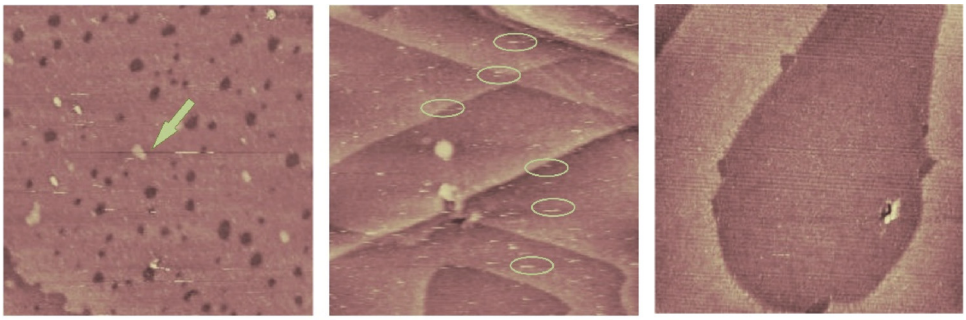

Fig. 1. Three typical kinds of defects of STM topography: (a) long stripe defects (pointed by arrow). (b) Short sparse stripe (circled by ellipses). (c) periodic noise (global).

Because of the difficulties of sample and probe preparation and the long period of scanning, getting a STM image is time consuming. And also, researchers usually need scanning many times to get an entire perfect image without any defects covering up the real morphologies. The original intention of this article is to introduce a restoration method for giving researchers quick hints of the real morphologies when the STM images have defects.

Many image processing methods have been introduced in STM image restoration and de-noising, such as, Sparse Coding (Oliveira et al., 2016), TV and Criminisi algorithms (Xian-guang et al., 2019) and so on. While all these algorithms relied on manual classification and manual positioning of defects. Moreover, the complexity and time consumption can be added along with the defects amount increasement and position randomness augment. Therefore, in this study, a novel method for STM image post-processing is provided. It combines with defects classification network which using DCNN and unique image processing algorithms. Using this method, STM images can be fast restored automatically by defects self-positioning and self-processing and the entire process minimize the manual intervention.

The rest of the paper is organized as follows. Section 2 provides the flow path and the theories of the whole automatic processing method including the classification work and the restoration work. Section 3 discusses the effectiveness of the whole processing method. Finally, Section 4 summarizes the conclusions.

2. Methods

2.1. Image processing strategy

As observed in Fig. 1, each kind of defect has its unique feature which has no relationship with the morphology presented. The valid restoration methods become diverse because of the specificity of each kind of defects which makes distinguishing defects separately necessary. Furthermore, on account of the independence between defect features and the content presented, classifying defects entirely by computer without manual works are possible. Therefore, the central idea of the developed algorithm consists of two parts:(1) classifying defects and marking all defect types. (2) self-positioning and self-processing of each marked defect type by different means according to appointed priority. The flowchart of the developed algorithm is shown in Fig. 2, and the various detailed steps involved in the algorithm are discussed in subsequent chapters.

2.2. Defects classification and marking

A STM image may contain more than one type of defect which makes defects recognition a multi-label learning problem. The key challenge of multi-label learning problems is the large size of the output space. As the types of label increases, the size of label sets grows exponentially (Zhang and Zhou, 2014). Thus, a solving method called cross-training which transform the defects classification problem into three independent binary classification problems is to be used (Boutell et al., 2004). Because of the irrelevance between the different defect labels on each image, the coexistence of other labels can be ignored when training one label(Zhang and Zhou, 2007). Then, how to set up and train the unique classification network for the three defects becomes the core problem.

On account of the difficulties in features extraction, traditional supervised machine-based learning methods, such as k-NN, SVM, need some extraction techniques (e.g., SIFT, HOG, GIST) (Zhang et al., 2018). Hence, the deep convolutional neural network (DCNN) which can extract features automatically and does not need hand designed features (Liu et al., 2019) is be chosen. The base structure of the proposed DCNN network contains 5 convolution layers and 2 fully connected layers as Fig. 3 presented. Because of that the features of the defects are tinny and unimpressive, the dimensionality of the whole image is too large by contrast. Thus, one pooling layer is added after each convolution layer to descend dimension of output features (Hu et al., 2015). The pooling layer can reduce the trained parameters and can automatically judge which features play key roles in the defects' classification. The detailed parameters are different according to the diverse features the three defects have.

2.2.1. Periodic noise classification network

Although the periodic noise is global, the features of it are weak relative to the diverse background morphologies. Thus, it's necessary to select appropriate size of the convolution kernel. Convolution kernel is also known as a receptive field. The pixels in the kernel will be weighted sum as a new pixel in the next layer, as the Fig. 4 shown. When the defects' size is small, if the kernel size is set too large, the characteristics of defects may be neglected during training. And also, when the stride is set large (even equals to the kernel size), if the defects are in middle of the kernel margin, the defects' characteristics may loss. So the kernel size of each five convolution layers is set to 3*3 to ensure the effect that features of periodic noise can be learned by the network and all strides of each five convolution layers are set to 1. Correspondingly, filters number are 128,128,128,64,64 respectively. All pooling layers are use max-pooling method and 2*2 kernel size. The nodes number of followed 2 fully connected layers are 1024 and 32. In the hidden layer section, each output will be nonlinearized by the Relu activation function which can reduce the calculation and improve convergence. The Relu activation can also reduce the interdependence of parameters which can prevent overfitting (Yarotsky, 2017). The output layer is a 1 node full-connected layer and activation function is Sigmoid. Thus, the output 1 represents pending image has periodic noise and 0 represents it does not have.

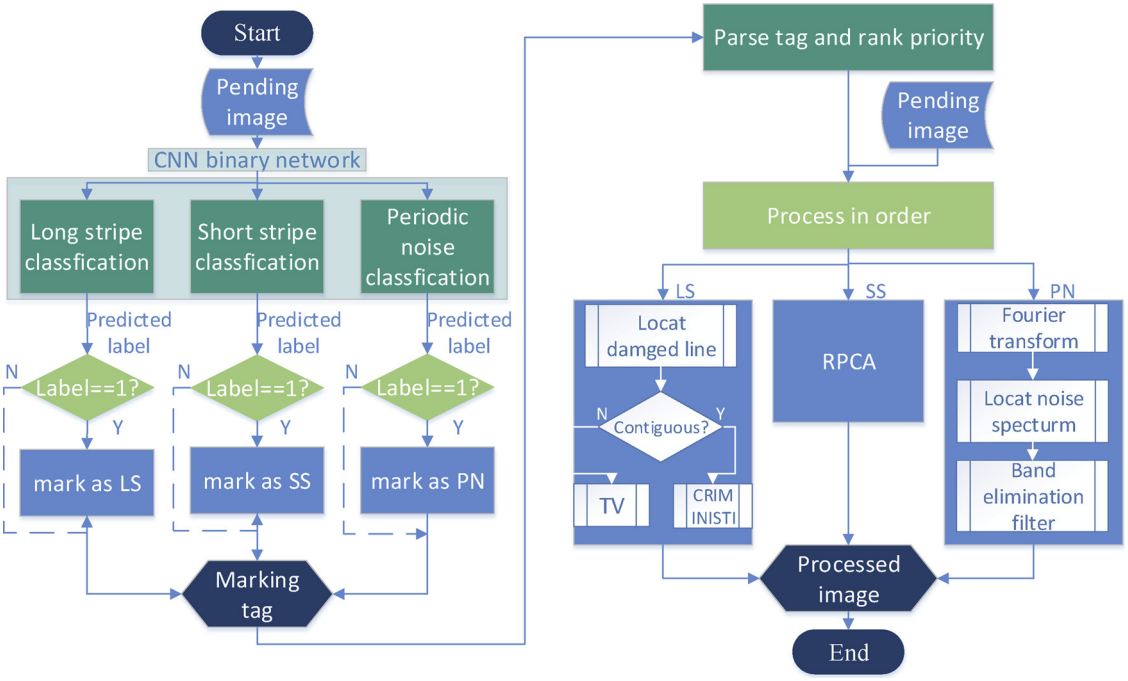

Fig. 2. Flowchart which showing the whole provided processing method. The left part is the flow of the defects classification and marking, the right part shows the details of the restoration of each kind of defects.

2.2.2. *Long stripe classification network*

Long stripe is local noise, so the evidence of its features is weaker than periodic noise. If using the same parameters of periodic noise classification network, the overfitting phenomenon, that the accuracy of training set rocket to nearly 100 % while the accuracy of validation set rises slowly or even declines, may appear in training. Thus, in order to avoid the network being trained to remember all the samples (the training set's accuracy is 100 % but the testing set's accuracy is very low), the size of the first full connected layer is reduced to 512 as shown in Fig. 3.

2.2.3. *Short sparse stripe classification network*

Short sparse stripe is also local noise, and the sparsity and randomness are higher than long stripe. Furthermore, on account of the tinny size of each stripe, the feature of short sparse stripe is the weakest among three defects. On account of that the short stripe is sparse, if the stride is small, the sum of each kernel's pixels may become similar and the sparse defects may loss its features during the training. In order retain small features during the convolution, the strides of the first three convolution layers are increased and the filters number change to 16, 32 and 64 as demonstrated in Fig. 3.

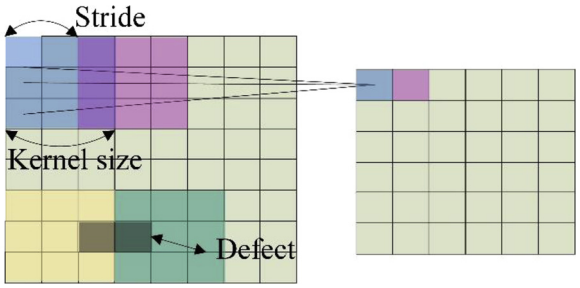

Fig. 4. The explanation of the parameter of convolution process. The stride represents the interval of kernels. The kernel size represents the dimension of the kernel matrix. When the stride is set equal to the kernel size and the small defect is in the margin of two kernel, the character of the defect for each kernel is very weak and may be neglected.

2.3. *Defects restoration methods*

What kind of defects a pending image contains was described by the classification network in Section 2.2. Thus, the following work is restoring the image in what way and in what priorities. Because the restoring methods for the three defects have slightly different side effects which may affect other defects restoration of pending images, the order

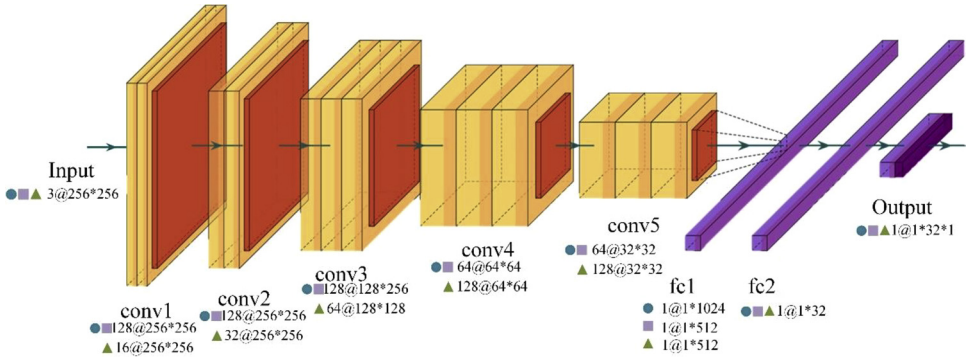

Fig. 3. The base structure of proposed DCNN binary network (conv represents the convolution layer, fc represent the connection layer). The detailed parameters are presented in the figure: ● represent the concrete parameters of the periodic noise binary network, ■ represent the concrete parameters of the long stripe binary network, ▲ represent the concrete parameters of the short stripe binary network. Expect for the conv1, each convolution layer is combined with a max-pooling layer. Expect for the output layer which activated by Sigmoid function, the result of each layer is activated by Relu.

of each process is important to ensure the restoration effect. First, periodic noise restoration may make the margin of the long stripes become a little blur, which may cause difficulties of their positioning. Second, short sparse stripes restoration uses a kind of low rank recovery algorithm which can eliminate the outliers of the image (not only the short sparse stripes but also the sparse components of other defects). Thus, the original character of the periodic noise and long stripes may be changed which make their restoration more difficult. Above all, we set that the periodic noise restoration should be after the long stripe restoration and the short sparse stripe restoration should be in the last. So the priority level of three defects is defined as Eq. 1:

$$LS > PN > SS \tag{1}$$

where LS represents long stripe, PN represents periodic noise, SS represents short sparse stripe.

2.3.1. Long stripe restoration

Long stripe defect is a kind of image damage whose main causes are pinpoint tinny shaking. Some studies have proposed some effective algorithms of image damages restoration for different types of damages.

Total Variation (TV) algorithm was proposed by Rudin & Osher in 1992 (Rudin et al., 1992),and was amended and used for image inpainting by Chan in 2002 (Chan and Zhou, 2002). The principle of TV is mentioned in the Supporting Information Part 1. Because of TV using the outside boundary information, this restoring method is effective only when the damage size is relatively small. Otherwise the restoration result will become blur in center section of marked pending region as Fig. 5 shown.

Criminisi algorithm is a global searching algorithm used widely in texture repairing. The principle of Criminisi is mentioned in the Supporting Information Part 2. Because of the globality of the searching and matching, when the pending area is smaller than the template, the restoring result may have pseudo textures, as Fig. 5.

To solve the shortcoming of the two algorithms and make the best of the two methods, (Xian-guang et al., 2019) proposed a method which combines the two in restoring STM image damages. While this method needs manual positioning and judging of the defects. Hence, a self-positioning, self-judging and self-restoring algorithm is proposed.

Through the analysis of the long stripe defects, a phenomenon is found that the texture differences between damaged rows and adjacent lines are much larger than that between undamaged rows. Thus, we proposed a novel index parameter called 'row gradient' (denoted by RG) which presents the sharpness of transition between two rows. The formula of RG is Eq. 2:

$$RG(x) = \sum_{i=0}^{n} \frac{(p(x-1,i) - p(x,i)) + (p(x,i) - p(x+1,i))}{2} \tag{2}$$

where x is the row of the image; n is the width of the image; p is the image matrix. As the Fig. 6 shown, the RG values of the damaged rows

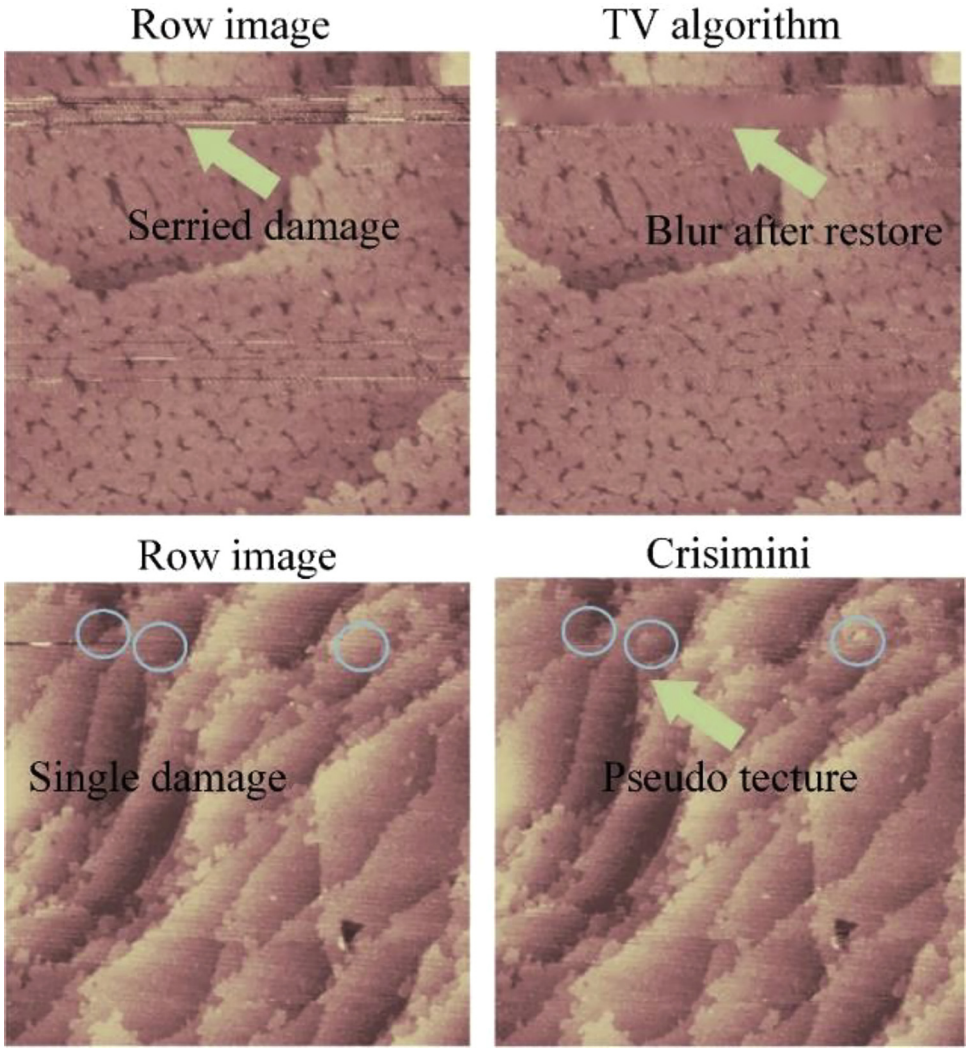

Fig. 5. Weaknesses of the TV and Criminisi algorithm. Image becomes blur when use TV to restore large area damage. Criminisi algorithm may make image have some pseudo textures when the damage area is small.

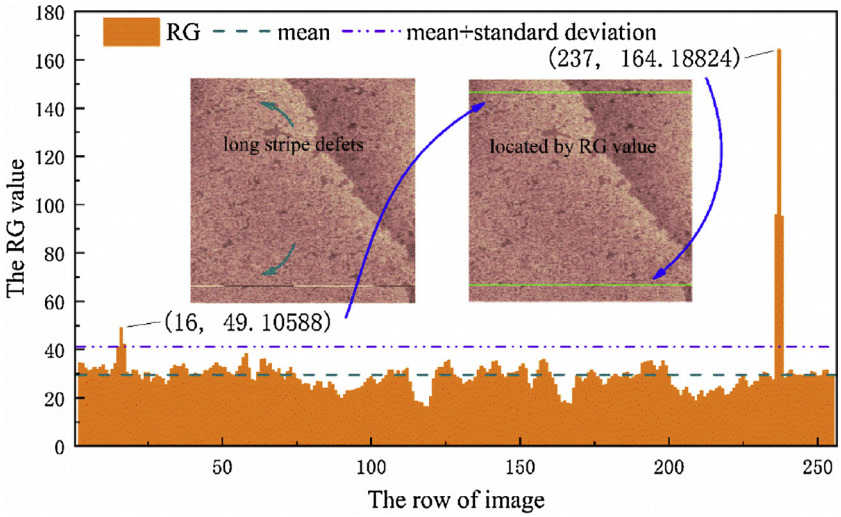

Fig. 6. Demonstration of how to use the RG value to locate the damaged line. The purple line (the upper peaked line) represents the mean of RG plus the standard deviation of RG. The rows (16th & 237th) whose RG value surpass the threshold correspond the damaged lines. (For interpretation of the references to colour in this figure legend, the reader is referred to the web version of this article.)

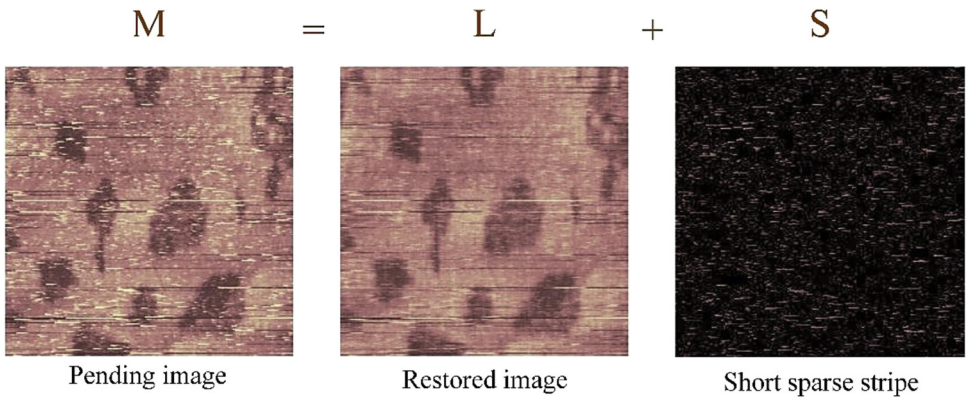

Fig. 7. the figure presents how the RPCA restore the short sparse stripe. The RPCA algorithm divides the row image into two matrixes, the S matrix includes the sparse outliers (short stripe) of the image, and the L matrix includes the remain low rank section. The L matrix is the image that restored by RPCA.

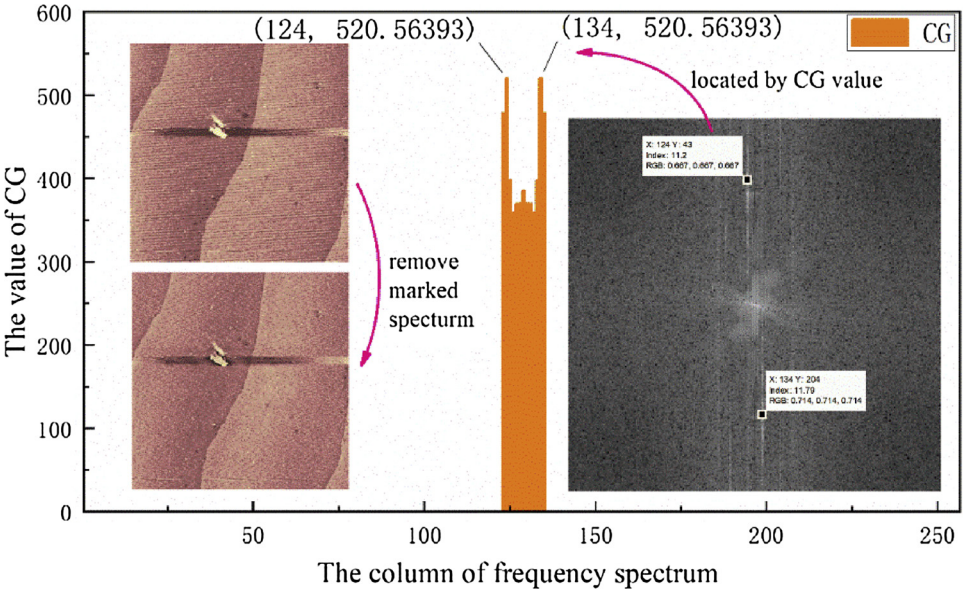

Fig. 8. Demonstration of how to use the CG value to locate the spectrum of the periodic noise. The marked centrosymmetric light lines (124th column & 134th column) are the periodic noise section of the spectrum which correspond the marked highest CG value from 123rd to 135th. Thus, the location of the periodic noise spectrum can be ensured by the CG value. As the left two image shown, after removing the located section of spectrum, the periodic noise is restrained well.

are prominently higher than others, and RG values of the rows above and under the damaged line are about half of damaged rows'.

Then, the core work is finding the suitable threshold value of RG to divide the damaged rows and undamaged rows. In one pending image, the majority of the rows are undamaged, thus the average of the RG nearly represents the datum RG value of undamaged rows. Also, the standard deviation of the RG can represent the extent of the RG augment of the damaged rows. Thus, the threshold value is defined as Eq. 3:

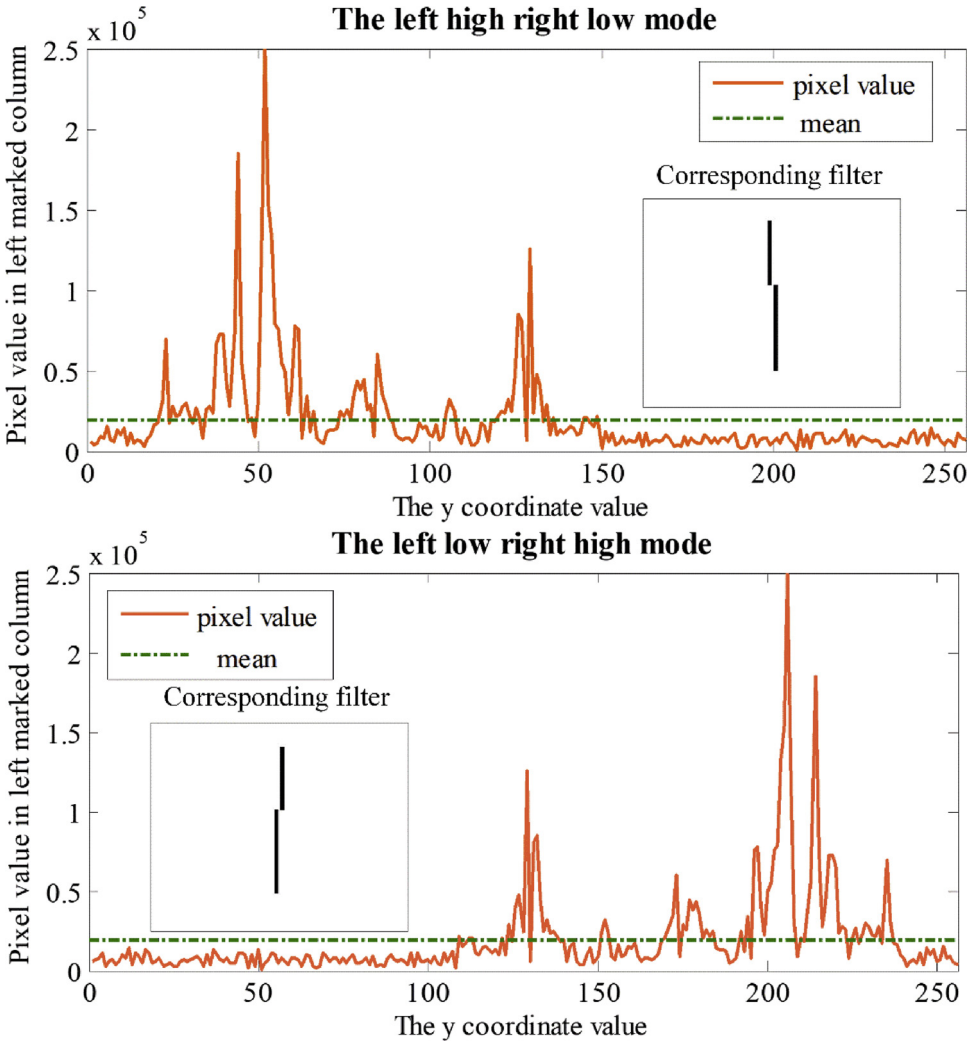

Fig. 9. Demonstrates of how to choose the corresponding filter to remove the periodic noise spectrum. When most of the pixels which are above the mean is distribute on the left, the filter mode is defined as 'left high right low' (above). On the contrary, when most of the pixels which are above the mean is distribute on the right, the filter mode is defined as 'left low right high' (below).

Table 1
The amount and distribution of the data set of three types of defects. The original part presents the PN/NE samples' distribution, the * mark represents the samples are comparative (have totally same morphology except for defects). The divided part present how the original data randomly divided into three sets (train set, valid set, test set).

Data Set Size	Original		Divided		
	PN	NE	Train	Valid	Test
Periodic Noise	170	174	281	23	40
Long Stripe	126* + 76	126* + 60	300	44	44
Short Stripe	233	204	300	69	68

Table 2
Augment method and augmented set size of three types of defects.

Data Augment	Train Set	Augment Method			Augmented Set
		Rotate	Zoom	Flip	
Periodic Noise	281	± 10°	±0.2 %	H/V	5708
Long Stripe	300	×	×	H	5216
Short Stripe	300	×	±0.1 %	H	5216

$$thr = \overline{RG} + \sigma RG = \frac{\sum_{x=1}^{n} RG(x) + \sum_{x=1}^{n} (RG(x) - \frac{\sum_{x=1}^{n} RG(X)}{n})^2}{n} \quad (3)$$

Expect for the rows that adjoin the damaged row, the pending rows can be marked as Fig. 6.

Then, the restoring method is chosen automatically through whether the damaged rows are intensive, the judge formula is Eq. 4:

$$\text{intensive flag} = \begin{cases} yes & \text{restoring by criminisi} \\ no & \text{restoring by TV} \end{cases} \quad (4)$$

To sum up, after the algorithm mentioned above, the pending image marked having long stripe defects can be restored automatically without any manual intervention.

2.3.2. Short sparse stripe restoration

Short stripe defects can be viewed as global sparse outliers, although they can also be viewed as local damage. Beside the sparse defects, the undamaged area of the pending image is identified as low-rank matrix. On this assumption, the restoring process becomes a work that recover the low-rank section of the pending image, namely separating M = L0 + S0 into the terms L0 and S0 (Candès et al., 2011). Although the problem is N-P hard, a super-duper solution to those low-rank and sparse decomposition problems was introduced by Emmanuel Cand´es

Table 3
The confusion matrix and the evaluation of three binary networks. ACC represents accuracy defined as (TP + TN)/Total, Precision is defined as TP/(TP + FP), Recall is defined as TP/(TP + FN), (TP: true positive, TN: true negative, FP: false positive, FN: false negative). F-1 represents the value of F-measure (when α= 1) which defined as $F_\alpha = \frac{(1+\alpha^2)Precision \times Recall}{\alpha^2 Precision + Recall}$.

Periodic Noise	Predicted				Evaluation Criterion			
		PN	NE	TOTAL	ACC	Precision	Recall	F-1
Actual	PN	20	2	22	92.500 %	95.238 %	90.909 %	93.023 %
	NE	1	17	18				
	TOTAL	21	19	40				

Long Stripe	Predicted				Evaluation Criterion			
		PN	NE	TOTAL	ACC	Precision	Recall	F-1
Actual	PN	23	2	25	91.489 %	92.000 %	92.000 %	92.000 %
	NE	2	20	22				
	TOTAL	25	22	47				

Short Stripe	Predicted				Evaluation Criterion			
		PN	NE	TOTAL	ACC	Precision	Recall	F-1
Actual	PN	37	4	41	92.063 %	97.374 %	90.244 %	93.674 %
	NE	1	21	22				
	TOTAL	38	25	63				

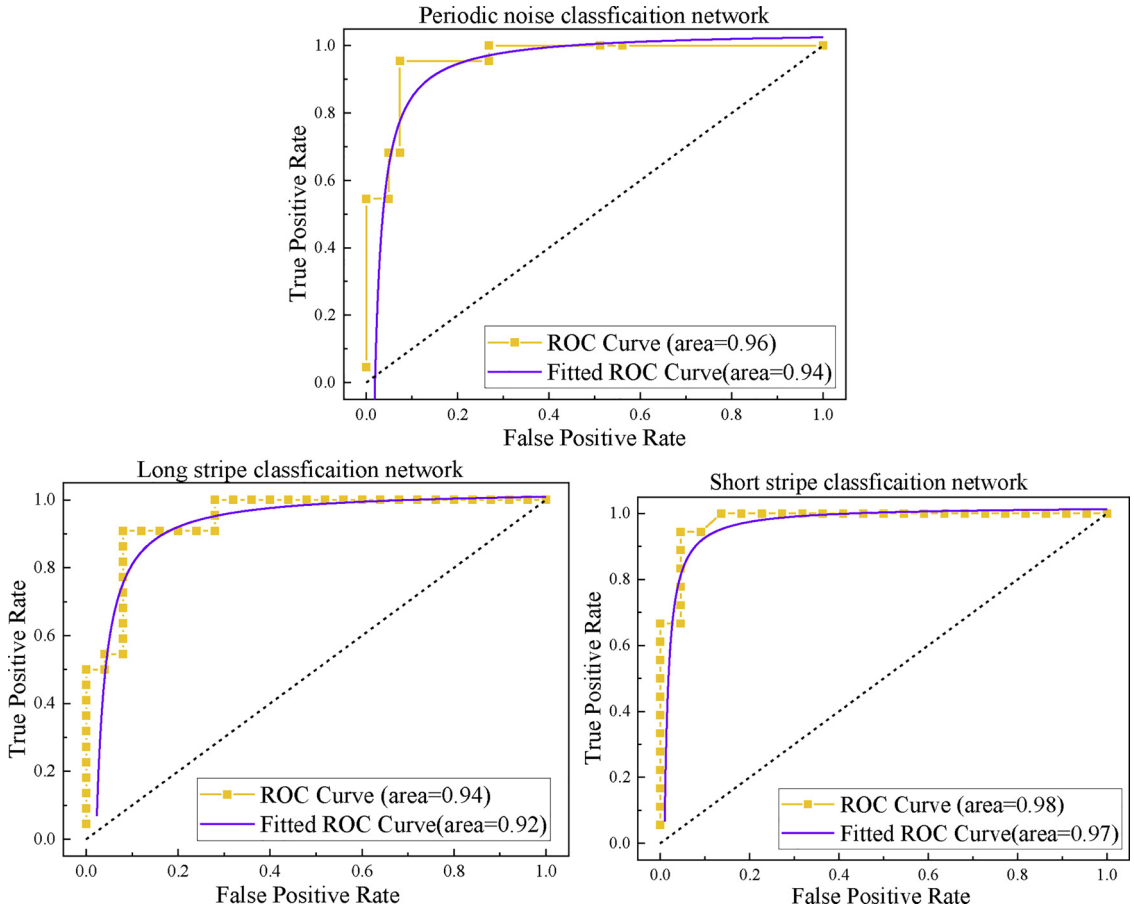

Fig. 10. ROC (receiver operating characteristic) curve and AUC (area under ROC curve) of three types of defects.

et al. in 2010 called Robust Principal Component Analysis (RPCA). In this method, the low-rank L0 and sparse S0 which generated data can be exactly recovered by solving a simple convex program (Candès et al., 2011):

$$\begin{aligned} &\text{minimize } \|\mathbf{L}\|_* + \lambda \|\mathbf{S}\|_1 \\ &\text{subject to} \mathbf{L} + \mathbf{S} = \mathbf{M} \end{aligned} \tag{5}$$

where $\|\boldsymbol{L}\|_* = \Sigma_y \sigma_i(\boldsymbol{L})$, $\|\boldsymbol{S}\|_1 = \Sigma_{ij} |\boldsymbol{M}_{ij}|$. This principle has been widely used in image processing and video processing (Bouwmans et al., 2018), and inspire applied work in image video analysis. On account of

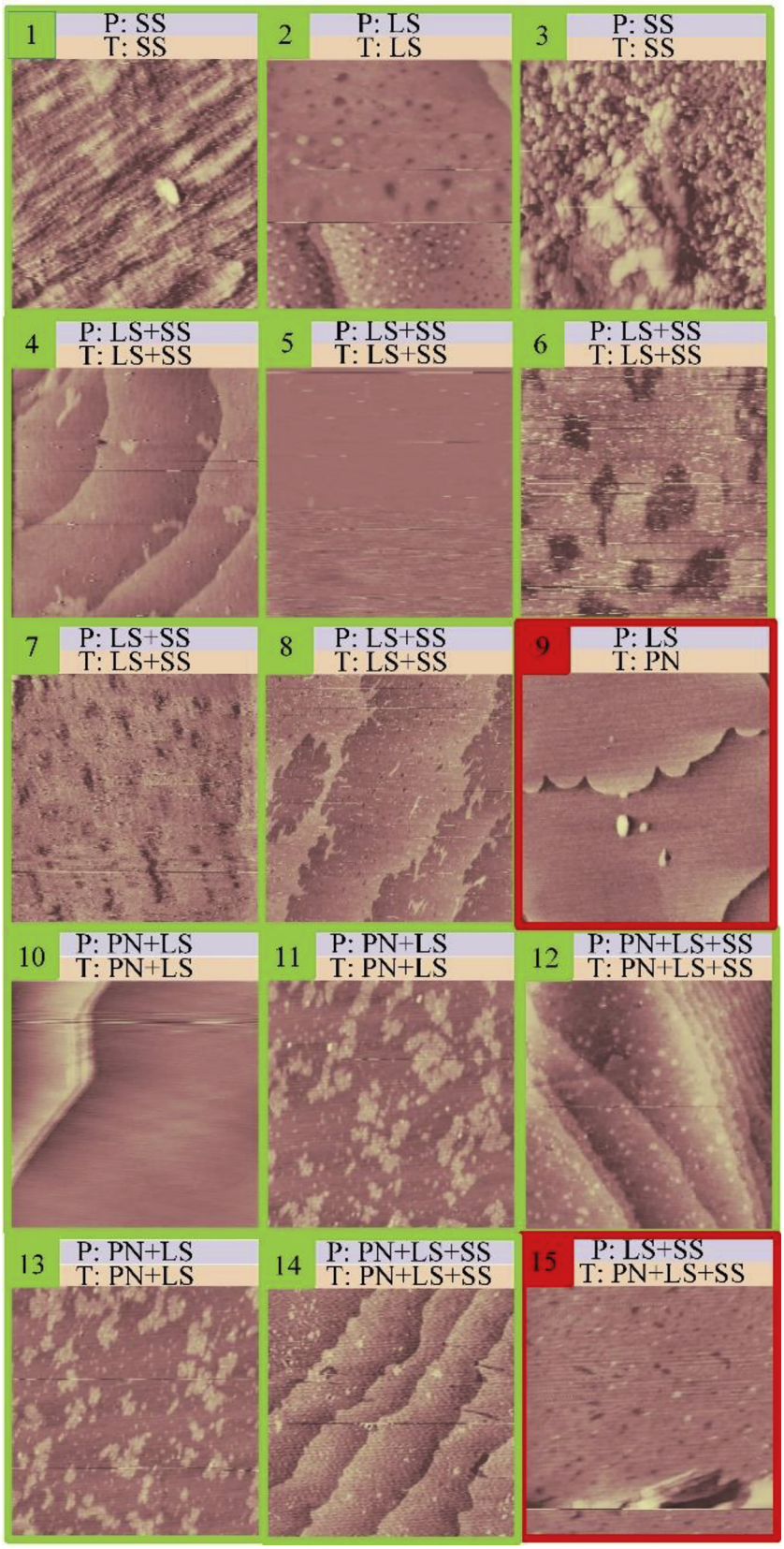

Fig. 11. The prediction on 15 new generated STM images by the trained classification network. label of each image is the true label tagged manually and label of each image is the predicted label by the classification (P: predicted, T: true, LS: long stripe, SS: short stripe, PN: periodic noise). The accuracy is shown by the rectangle on the top left corner. (green represents correct, red represents incorrect). (For interpretation of the references to colour in this figure legend, the reader is referred to the web version of this article.)

that the short sparse stripe defects can be viewed as the S matrix, restoring this kind of defects can be solved by RPCA as Fig. 7 presented.

2.3.3. Periodic noise restoration

Periodic noise is usually hard processed directly in time domain although it has obvious periodic feature. Because of the ability of the Fourier transform to convert a complex convolution operation in the

Table 4
the effectiveness of three restoration algorithms. The judgement 'good' represents the defects are restored visually well with little residue and pseudo stripe. The judgement 'bad' represents the defects partly remain or some side effects are introduced. Part of the samples are shown in the Supporting Information Part 3.

Image Restoration	Restoration Result			Success Rate
	total	good	bad	
Periodic Noise	50	48	2	96%
Long Stripe	50	46	4	92%
Short Stripe	50	49	1	98%

spatial domain into a simple product operation in the frequency domain, frequency domain filtering has been widely used in periodic de-noising of images. While, the shape and location of the filter determine the effect of de-noising, thus positioning the frequency domain that to be removed is a very important task. The Fourier transform of two-dimensional image $f(x, y)$ is Eq. 6:

$$F(u, v) = \frac{1}{MN} \sum_{x=1}^{M-1} \sum_{y=0}^{N-1} f(x, y) e^{[-j2\pi(\frac{ux}{M} + \frac{vy}{N})]} \tag{6}$$

The frequency of periodic noise is two light vertical lines centrosymmetric distributing around the center of the spectrogram as the Fig. 8 presented. Also, analytically the distance between the light line and the center column is range from 1pixels to 6 pixels. The light lines' position can be ensured by an index parameter called 'column gradient' (denoted by CG) which is defined like the way mentioned in 2.3.1, as the Eq. 7.

$$CG(x) = \sum_{i=0}^{n} \frac{(p(i, x-1) - p(i, x)) + (p(i, x) - p(i, x+1))}{2} \tag{7}$$

So, the column which has the highest CG value is the light line which contain the spectrogram of the periodic noise, as shown in Fig. 8.

After ensuring the light lines' position, the next task is to estimate whether the light lines are distributing as 'left high right low' mode or 'left low right high' mode. Through analyzing the pixels' values in the left light line in Fig. 9, when the distribution mode is 'left high right low, the average of the 1˜128 pixels is obvious higher than that of the 129–256 pixels, vice versa.

Then, after ensuring the distribution of the light line, choosing a suitable filter can restore the periodic noise of the pending image

3. Results and discussion

The processed STM images were generated from 2007 to 2015 by the STM module of NanoScope®E produced by Digital Instruments department which total number is around ten thousand. The image size is 256*256 which has RGB three channels. It is analyzed and found that long stripe, short sparse stripe, periodic noise which are approximately occupy 33 %, 28 %,22 % respectively.

3.1. Classification results

Through manual recognition and tagging, we collect three original data sets as Table 1 shown. The positive samples (containing corresponding defects) and negative samples (not containing corresponding defects) are roughly equally distributed. However, in the long stripe defect data set, we collect 126 positive samples and 126 negative samples which have totally same morphology except for long stripes in order to help the network study the characteristics of long stripes. Then, after shuffling the data set, respectively divide the dataset into three sets for training, validating and testing.

Then, in order to get good classification performance, we make some minor alterations such as flips, zooming and rotations to the existing training data sets as Table 2 shown (Teramoto et al., 2017). Because of the periodic noise is global noise and the characteristics of it are sensitive to direction, we randomly rotate the data in the range of ± 10° and zoom the data in the range of ± 0.2 % and flip the data both horizontally and vertically. While, to the short stripe and long stripe, on account of the locality and the sensibility of direction, we only use the horizontal flip and only zoom the short stripe data in the range of ± 0.1 %. Through these minor changes, the training data amount of each set is increased to around 5500 which is more proportional to the parameters of the net.

After the training data's preparation, we use the augmented training data sets to train the correspondent binary networks. And the accuracy of one validating data set indicates the degree of the training correspondingly. We test each binary network in correspondent testing data set, and the resulting confusion matrix of each binary network is shown in Table 3. The accuracies of the three binary networks are respectively 92.500 %, 91.489 % and 92.063 %. We also use the precision value, recall value and f-measure (a = 1) to evaluate the binary networks. Fig. 10 presents the three binary networks' ROC (receiver operating characteristic) curves and the AUC (area under ROC curve) values. Putting all the evaluation indexes together, the three binary networks work well separately in each classifying work.

In order to verify the universality of the classification net, we choose 15 image samples which are newly generated by the STM to validate the accuracy of the classification. As the Fig. 11 shown, the true label which was tagged manually is attached in the rectangle at the top of each image, and the predict label is attached in the rectangle. The color of the rectangle at the top left corner represent the correctness of the classification (green represent correct, red represent incorrect). Among the 15 test samples, 13 images are classified correctly, 2 images have little deviation on the prediction, which are the 9th and 15th respectively. Through analyzing, the periodic noise of the 9th image is very sharp and the single stripe of the noise is similar as a long stripe defect, which may cause the mistake of the prediction. The periodic noise of the 15th image is slightly blurred which may lead to the mistake.

The overall results indicated that the deep convolutional neural network provided above have a quite well performance in the defects classification and prediction work.

3.2. Restoration result

Table 4 indicates the effectiveness of the provided restoration methods mentioned before. Three provided algorithms respectively process 50 images which have typical corresponding defects, and only a few of images are not restored good remaining some defects. The integral success rate of restoration is around 95 % (± 3%).

Fig. 12 presents the entire restoring process without any manual intervention. The No.1 topography (CPI/Pd(monolayer)/Au) is correctly predicted by the network as LS and SS. It is restored automatically by the long stripe restoration algorithm (self-locating TV& CRISMINI) and short stripe restoration algorithm (RPCA). No.2 (Autip1/Pd/Au (111)) and No.3 (Pd(monolayer)/Au) are both predicted as NP and LS. After the process, the long stripes are restored well and the periodic noise are repressed obviously not entirely (remain little slight grains). No.4 (4CPI/Pd(monolayer)/Au) is predicted as NP, and the periodic noise is removed well.

4. Conclusions

We have proposed a new fully-automatic method for STM post-processing combing CNN classification network and three specific restoring algorithms. In the traditional post-processing for STM, the complexity of the morphologies and the defects make the restoration a complex and time-consuming thing which requires a lot of human

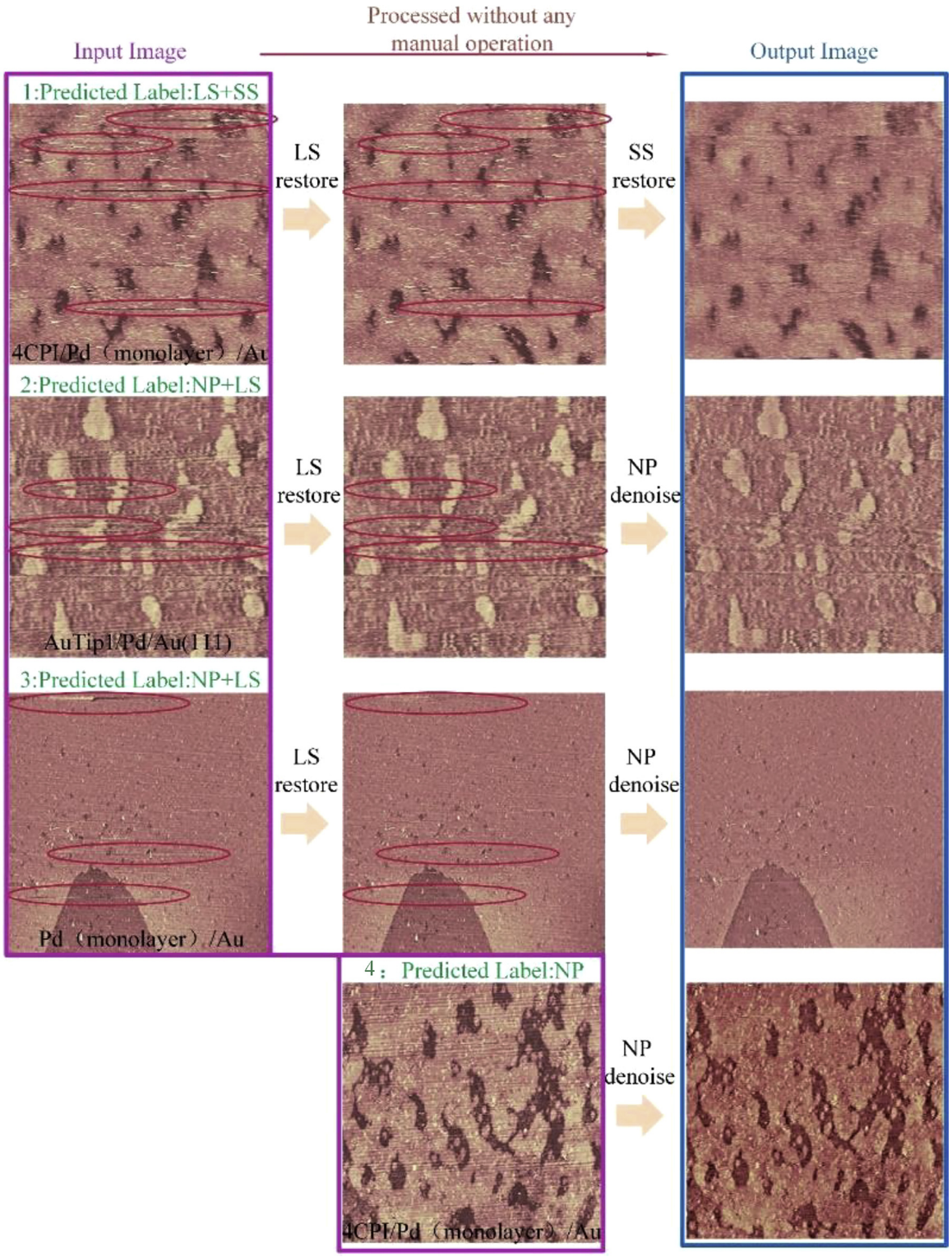

Fig. 12. This figure demonstrates visually the process and effectiveness of the whole restoration method. The processed image is the morphology of (CPI/Pdmonolayer/Au) (no.1), Autip1/Pd/Au(111) (no.2), Pd(monolayer)/Au (no.3), 4CPI/Pd(monolayer)/Au (no.4), where CPI represents P-chloro-isonitrile benzene molecule and Autip1 represents using the Au tip 1 to scanning.

intervention. The method proposes a new idea that combines a deep learning classification network and traditional image processing algorithms. This combination provides a model for combing several algorithms for specific defects into a universal restoration method. It not only overcomes the limitation of restoring algorithms for specific defects but also reduces the manual intervention during the restoring. The processed results demonstrate the effectiveness of the method adequately. The software can process image in seconds automatically without any manual intervention, the processed results are shown in an individual form as hints only for the researchers (the original data is always stored). The print screen of the software is in part 6 of the supporting information.

Further research should be focused on expanding the kinds of defects that can be handled and on how to change the process order adaptively to get the best process result. The new process model can make further work focus on particular defects' positioning and restoration instead of focusing on finding a universal restoring method. And also, on the current method, the order of process is determined by prior experience and can't be changed in different conditions. Future work could weight each label of defects and train a network to determine the order of the restoration process dynamically.

Acknowledgement

This work was supported by the National Nature Science Foundation of China (Nos: 21874133, Nos:21974118), the National Nature Science Foundation of China (Major Program, Nos: 21790354) and State Key Laboratory of Physical Chemistry of Solid Surfaces, Xiamen University.

Appendix A. Supplementary data

Supplementary material related to this article can be found, in the online version, at doi:https://doi.org/10.1016/j.micron.2019.102798.

References

Binnig, G., Rohrer, H., 1987. Scanning tunneling microscopy-from birth to adolescence. Rev. Mod. Phys. 59, 615–625.
Binnig, G., Rohrer, H., Gerber, C., Science, E.W.J.S., 1983. (111) facets as the origin of reconstructed Au(110) surfaces. Surf. Sci. 131 L379—L384L384.
Binnig, G., Rohrer, H.J.S.S., 1983. Scanning tunneling microscopy. Surf. Sci. 152, 17–26.
Boutell, M.R., Luo, J., Shen, X., Brown, C.M., 2004. Learning multi-label scene classification. Pattern Recognit. 37, 1757–1771.
Bouwmans, T., Javed, S., Zhang, H., Lin, Z., Otazo, R.J.P.o.t.I, 2018. On the applications of robust PCA in image and video processing. Proc. IEEE 106, 1427–1457.
Candès, E.J., Li, X., Ma, Y., Wright, J., 2011. Robust principal component analysis? J. ACM 58, 1–37.
Chan, T.F., Zhou, H.M., 2002. Total variation improved wavelet thresholding in image compression. International Conference on Image Processing.
Hu, W., Huang, Y., Wei, L., Zhang, F., Li, H., 2015. Deep convolutional neural networks for hyperspectral image classification. J. Sens. 2015, 1–12.
Ji, T.Y., Lu, Z., Wu, Q.H., 2007. Optimal soft morphological filter for periodic noise removal using a particle swarm optimiser with passive congregation. Signal Processing 87, 2799–2809.
Kelty, S.P., Lieber, C.M.J.J.C., 1989. Scanning tunneling microscopy investigations of the electronic structure of potassium-graphite intercalation compounds. J. Phys. Chem. 93, 5983–5985.
Kumar, A., Telesio, F., Forti, S., Al-Temimy, A., Coletti, C., Serrano-Ruiz, M., Caporali, M., Peruzzini, M., Beltram, F., Heun, S., 2018. STM study of exfoliated few layer black phosphorus annealed in ultrahigh vacuum. 2d Mater. 6.
Li, H., Hui, P., Shu, N., 2010. Study on suppressing White noises and periodic narrow bandwidth noise of PD by vertically invariant gray-level morphological filter. International Conference on E-Product E-Service. E-entertainment.
Liu, X.L., Zhang, R.J., Meng, Z.J., Hong, R.C., Liu, G.C., 2019. On fusing the latent deep CNN feature for image classification. World Wide Web 22, 423–436.
Moallem, P., Masoumzadeh, M., Habibi, M., 2013. A novel adaptive Gaussian restoration filter for reducing periodic noises in digital image. Signal Image Video Process. 9, 1179–1191.
Nguyen, H.A., Banerjee, P., Nguyen, D., Lyding, J.W., Gruebele, M., Jain, P.K., 2018. STM imaging of localized surface plasmons on individual gold nanoislands. J. Phys. Chem. Lett. 9, 1970–1976.
Oliveira, J.P., Bragança, A., Bioucas-Dias, J., Figueiredo, M., Alcácer, L., Morgado, J., Ferreira, Q., 2016. Restoring STM Images Via Sparse Coding: Noise and Artifact Removal.
Rosei, F., Schunack, M., Naitoh, Y., Jiang, P., Gourdon, A., Laegsgaard, E., Stensgaard, I., Joachim, C., Science, F.B.J.P.i.S, 2003. Properties of large organic molecules on metal surfaces. Prog. Surf. Sci. 71, 95–146.
Rudin, L.I., Osher, S., Fatemi, E., 1992. Nonlinear total variation based noise removal algorithms. Phys. D 60, 259–268.
Sur, F., Grédiac, M.J.J.I., 2015. Automated removal of quasiperiodic noise using frequency domain statistics. J. Electron. Imaging 24 013003-013003.
Tapaszto, L., Dobrik, G., Lambin, P., Biro, L.P., 2008. Tailoring the atomic structure of graphene nanoribbons by scanning tunnelling microscope lithography. Nat. Nanotechnol. 3, 397–401.
Teramoto, A., Tsukamoto, T., Kiriyama, Y., Fujita, H., 2017. Automated classification of lung Cancer types from cytological images using deep convolutional neural networks. Biomed Res. Int. 2017, 4067832.
Voelker, M.A., Hameroff, S.R., He, J.D., Dereniak, E.L., Weiss, L.B.J.J.M., 1988. STM imaging of molecular collagen and phospholipid membranes. J. Microsc. 152, 557–566.
Xian-guang, F., Xiao-dong, W., Yu-xin, C., Xin, W., 2019. Image processing for three defects of topography images by SPM. Chemom. Intell. Lab. Syst. 185, 12–17.
Yarotsky, D., 2017. Error bounds for approximations with deep ReLU networks. Neural Netw. 94, 103–114.
Zhang, M.-L., Zhou, Z.-H., 2007. ML-KNN: a lazy learning approach to multi-label learning. Pattern Recognit. 40, 2038–2048.
Zhang, M.-L., Zhou, Z.-H., 2014. A review on multi-label learning algorithms. IEEE Trans. Knowl. Data Eng. 26, 1819–1837.
Zhang, M., Li, W., Du, Q., 2018. Diverse region-based CNN for hyperspectral image classification. IEEE Trans. Image Process. 27, 2623–2634.